Problem Chosen	2026 MCM/ICM Summary Sheet	Team Control Number
A		2627379

TTE prediction model for smartphone lithium-ion batteries considering aging mechanisms and system feedback

summary

Under high load, low temperature, and aging conditions, smartphones often suffer from inaccurate time-to-empty (TTE) prediction and sudden shutdowns. To examine this issue, we propose a continuous-time differential-algebraic equation (DAE) model that captures the feedback between power demand and terminal voltage.

The model includes electrochemical dynamics and voltage hysteresis, while aging is reflected through capacity fade and internal resistance growth. Temperature effects are considered by allowing the resistance to vary with temperature through an Arrhenius-type relationship. A closed-loop power control formulation is used, so the load power is no longer prescribed in advance but depends on the battery state. As a result, the discharge process is treated as a constrained DAE system.

From the simulations, we observed that TTE may drop by as much as 81.5% under heavy load, with a further reduction of about 31.2% in cold environments. By examining the power balance, we find that sudden shutdown occurs when a saddle-node bifurcation is reached. A separate sensitivity check suggests that changes in internal resistance have roughly three times more influence on TTE than capacity fade. These results help explain unexpected shutdowns in aged batteries and may serve as a practical basis for battery-aware power management.

Keywords: Lithium-ion battery; Time-to-empty (TTE) prediction; Differential-algebraic equation (DAE); Voltage collapse; Saddle-node bifurcation.

Content

1. Introduction

1.1 Background

Modern smartphone power management is constrained not only by electrochemical energy storage, but also by nonlinear positive feedback between load power demand and terminal voltage.Under low-temperature and aging conditions, the internal resistance R_0 increases significantly, rendering the power balance equation $P=V \cdot I$ algebraically constrained. When batteries fail to meet instantaneous load power demands, the system crosses the boundary of the physically feasible region, leading to transient voltage collapse. This paper constructs an Index-1 differential-algebraic equation (DAE) framework to characterize the transition from steady operation to power infeasibility.

The assumptions made by the traditional Coulomb counting method and the open-loop equivalent circuit model are as follows.

In practical smartphone operation, these implicit assumptions break down under the combined effects of aging, low temperature, and aggressive power demand.

The resulting challenge is a strongly coupled multi-physics system in which electrochemical aging, thermal dynamics, and operating-system-level power feedback jointly determine the feasibility of power delivery.

1.2 work

To address this problem, we develop a continuous-time differential-algebraic equation (DAE) model incorporating state-of-health (SOH), voltage hysteresis, and closed-loop power control. The proposed model enables accurate prediction of time-to-empty (TTE) and voltage collapse thresholds.

The model simultaneously characterizes discharge duration, power feasibility boundaries, and the evolution of the safe operating area (SOA) under aging.

Our main work is as follows:

(1)Development of a multi-physics coupled DAE model integrating electrochemical dynamics, thermal effects, and cycle-induced aging.

(2) Explicit modeling of operating-system-level thermal throttling and voltage protection as implicit algebraic constraints, forming a closed-loop battery–load system.

(3) Dynamic stability analysis showing that transient shutdown corresponds to a saddle-node bifurcation on the discriminant manifold, enabling quantitative characterization of the safe operating area.

(4) Validation using NASA battery aging datasets, revealing the high sensitivity of TTE to internal resistance growth under low-temperature aging conditions.

2. Problem Analysis

2.1 Data analysis

Aging datasets (B0005, B0006, B0007, B0018) from the NASA Prognostics Data Repository were analyzed to characterize degradation variability under repeated cycling.The data show substantial dispersion in degradation behavior among cells with similar initial states after approximately 150 cycles.

For example, capacity fade ranges from 7.71% (B0018) to 41.75% (B0006) over comparable cycle counts.

In addition, internal resistance increases nonlinearly with aging and becomes the dominant contributor to terminal voltage loss near end-of-discharge, especially at low temperatures.

Accordingly, bounded stochastic perturbations and square-root aging laws are introduced to capture variability in capacity fade and resistance growth.

2.2 Analysis of question one

_For this reason, time-to-empty is better treated as the point where the constrained DAE process can no longer continue.

Under power-controlled loads, battery current becomes an implicit algebraic variable rather than an independent input.

As SOC decreases or resistance increases, the system approaches a discriminant boundary beyond which no physically feasible current solution exists.

Operating-system-level throttling acts to delay violation of this feasibility boundary by reducing power demand.

Consequently, TTE must be formulated as a termination problem of a DAE system rather than as simple charge integration.

3. Symbol and Assumptions

3.1 Symbol Description

The following is the explanation of the main symbols in this article.

Table 1 Symbol Explanation

Symbol	Definition	Unit
SOC(t)	State of Charge	Dimensionless 01
$V_{C1}(t)$,$V_{C2}(t)$	Polarization Voltages	V
H(t)	Hysteresis State	Dimensionless 11
T(t)	Battery Core Temperature	K
$I_{batt}(t)$	Discharge Current	A
$V_{term}(t)$	Terminal Voltage	V
V_{OCV}	OCV with Hysteresis	V
V_{eq}	Equilibrium Potential	V
R_0,R_1,R_2	ohmic/rapid/polarization slow polarization internal resistance	Ω
C_1,C_2	Polarization Capacitances	F
$Q_{max}(N_{cyc})$	Maximum available capacity in the current loop	Ah
N_{cyc}	equivalent cycle number of battery	Dimensionless
$P_{base}(t)$	system base power requirement	W
$P_{req}(t)$	actual load power after throttling	W
λ(V,T)	system power feedback throttling factor	Dimensionless 01
η_{pmic}	Power Conversion Efficiency	Dimensionless 01
mC_p	Total Heat Capacity	J/K
hA	Heat Transfer Coefficient	W/K
T_{amb}	Ambient Temperature	K
E_a	Activation Energy	J/mol
TTE	residual discharge time	min

3.2 Fundamental Assumptions

1. Total parameter and uniformity: The battery is regarded as a total system, and the distribution of internal temperature, concentration and electrochemical state is assumed to be uniform at the scale of a single cell. This assumption is reasonable for a single smartphone cell operating at medium or low discharge rates (≤2C).

2. Dual aging mechanism: Battery degradation consists of "calendar aging" (neglected) and "cycle aging", primarily manifested as increased internal resistance due to SEI film thickening and capacity fade caused by active lithium loss.

3. Normal distribution of individual variations: The initial parameters (R_0, Q_{n0}) of batteries within the same batch follow a normal distribution $N(\mu, \sigma^2)$. Thus, the variability in initial capacity and internal resistance among batteries of the same batch is modeled using a normal distribution disturbance term.

The stochastic perturbations are introduced solely to reflect manufacturing variability and are not treated as random variables for inference, but as bounded uncertainty terms constrained by empirical degradation envelopes.

1. **Separation of Scales and Quasi-static Approximation:**

The timescale of capacity degradation and resistance growth (cycles/months) is several orders of magnitude larger than that of a single discharge event (minutes/hours). Consequently, aging-dependent parameters (Q_{max},R_{aging}) are treated as quasi-static constants during the TTE prediction interval [0,t_{end}]. They are initialized as functions of N_{cyc} at t=0 and remain invariant during the integration of the DAE system.

2.Assumption for hierarchical shutdown logic:Soft Shutdown：

The system activates power-saving mode (power restriction) when theV_{term}≤3.4V ;

Hard Cutoff: When the V_{term}≤3.0V or power collapse occurs, that is, when there are no real roots in the algebraic constraints, forced power cut-off is implemented;

In the proposed model, hard cutoff is triggered either by voltage protection or by the loss of feasibility of the algebraic power constraint.

4. Mathematical Modeling

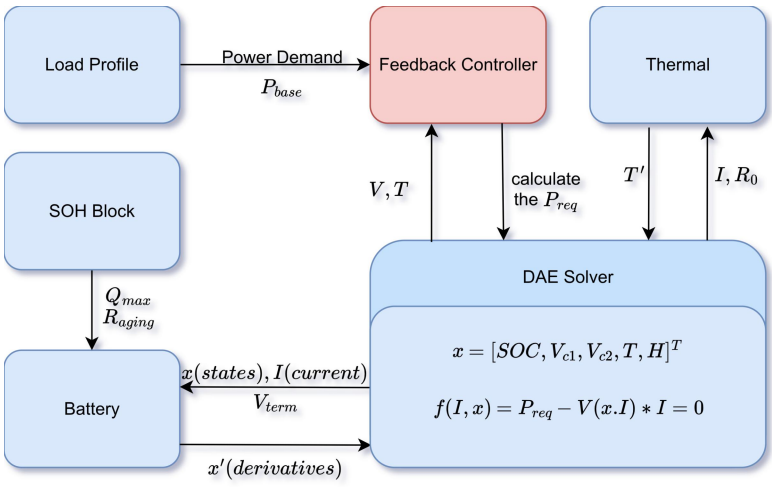

Figure 4-0. Architecture of the coupled DAE-based battery discharge model with aging, thermal dynamics, and closed-loop power feedback.

Electrical dynamics, thermal evolution, aging states, and system-level feedback are bidirectionally coupled, producing intrinsic algebraic loops between terminal voltage,

current, and power demand. Consequently, the system cannot be represented by a pure ODE and must be formulated as a DAE system.

Define system state vector:

$$\mathbf{x}(t)=[SOC(t),V_{C1}(t),V_{C2}(t),T(t),H(t)]^T \quad (1)$$

4.1 submodule 1: Parametric models that consider aging & individual differences

Before the simulation begins, the physical parameters of the current battery are determined based on its cycle count N_{cyc} and the individual variation factor δ .

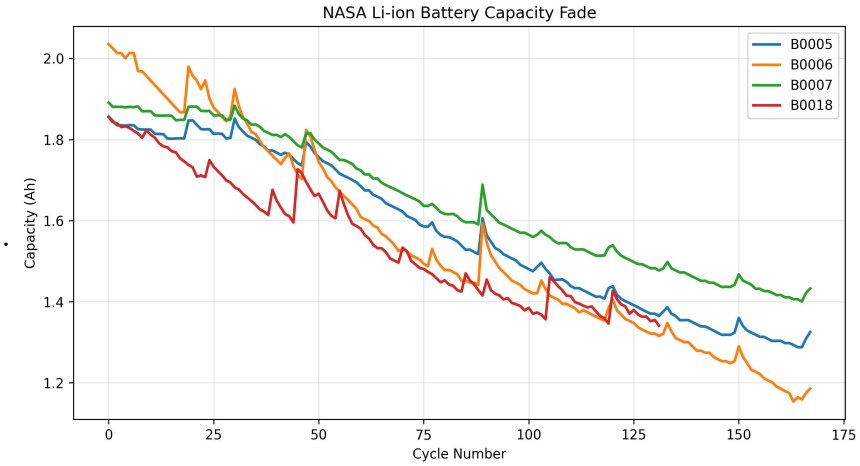

Figure 4-1 Capacity degradation trajectories of four lithium-ion cells from the NASA battery aging dataset.

Despite similar initial capacities, substantial dispersion in degradation rates is observed, motivating the introduction of cycle-dependent aging parameters and bounded uncertainty in the proposed model.

Aging parameters are constrained using NASA lithium-ion battery aging datasets (B0005–B0018).

Table 1 Capacity Degradation of Lithium-ion Batteries in NASA Aging Dataset

Battery	Cycles	Capacity Fade
B0005	168	28.62%
B0006	168	41.75%
B0007	168	24.25%
B0018	132	7.71%

These values are mainly used to limit the range of aging-related parameters in the model.

A.Capacity decay: Follows the square root law of SEI film growth:

$$Q_{max}(N_{cyc})=Q_{design}\cdot\ (1+\delta_Q)\cdot\ \left(1-\alpha_{sei}\sqrt{N_{cyc}}\right) \quad (2)$$

Here,δ_Q~ N(0,0.02) represents the individual capacity variation.

The square-root law is applied at the cycle level and does not imply continuous-time differentiability of capacity with respect to time. A lower bound is imposed on Q_{max} to prevent nonphysical negative capacity during long-term extrapolation. The parameter α_{sei} is calibrated such that $\alpha_{sei}\in[0.018,0.032]$ ensuring consistency with empirical degradation trajectories.

B. Internal resistance growth: The internal resistance increases linearly or exponentially with the number of cycles (depending on the chemical system; here, a linear approximation is used):

$$R_{aging}(N_{cyc})=(1+\beta_{res}N_{cyc})\cdot\ (1+\delta_R) \quad (3)$$

Here,δ_R~ N(0,0.03) represents the individual impedance variation.

Empirical studies on the dataset indicate that, experimental observations indicate that the effective DC internal resistance increases monotonically and can be approximated by a linear function. Therefore, a linearized aging model is adopted to balance physical fidelity and numerical tractability.

4.2 submodule 2: Closed-loop load and feedback control

To better reflect real smartphone behavior, the load is not treated as a constant, but changes with voltage and temperature feedback.

A. Base Power Demand:

$$P_{base}(t)=\frac{1}{\eta}\left(P_{disp}(t)+P_{cpu}(t)+P_{net}(t)\right) \quad (4)$$

B. System Throttling:

Introduce the regulation factor $\lambda(t)\in[0,1]$ to simulate the power management logic:

$$\lambda(t)=\min\left(\underbrace{\frac{1}{1+e^{(T-45)/2}}}_{\text{Thermal Throttling}},\ \underbrace{\tanh(k_v(V_{term}-3.0))}_{\text{Low Voltage Throttling}}\right) \tag{5}$$

$(T-T_{crit})$, $T_{crit}=45^{\circ}$ C, Temperature is expressed in degrees Celsius in the throttling logic for consistency with system-level thermal limits. It can be described as a soft handover function

$$\lambda(V)=\frac{1}{2}\left[1+\tanh\left(\frac{V-V_{crit}}{\epsilon}\right)\right] \tag{6}$$

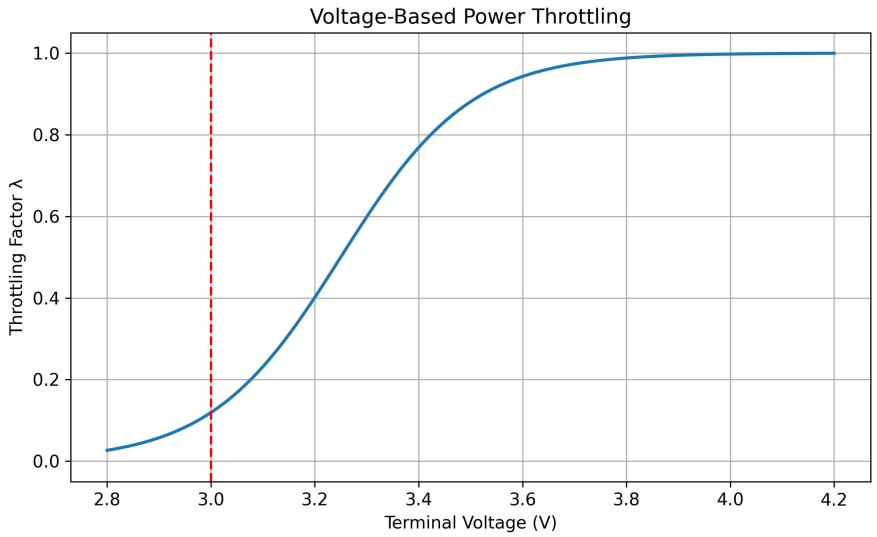

Figure 4-2. Voltage-Based Power Throttling.

The throttling function is not required to be smooth everywhere, as it represents discrete system-level power management logic rather than intrinsic electrochemical dynamics.

Actual load: The actual load powerP_{req} is a implicit function of voltage and temperature:$P_{req}(t)=P_{base}(t)\cdot\ \lambda(t)$, or $P_{req}=P_{base}\cdot\ \lambda(V,T)$.

4.3 submodule 3: Electrochemical Dynamics

A. Capacity-normalized SOC dynamic equation

$$\frac{dSOC}{dt}=-\frac{I_{batt}(t)}{Q_{max}},\qquad Q_{max}\text{expressed in Coulombs (As)} \tag{7}$$

B. OCV model with lag

The electrochemical dynamics are represented using a capacity-normalized SOC equation, an OCV model with hysteresis, and a dual-RC polarization structure.

$$V_{OCV}(SOC,H)=V_{eq}(SOC)+M(SOC)\cdot H(t) \tag{8}$$

The OCV curve is treated as an empirical monotonic function calibrated from typical smartphone Li-ion cells, rather than a chemistry-specific equilibrium potential.

Dynamic equation of lagged term:

$$\frac{dH}{dt}=-\kappa|I_{batt}|(H-\mathrm{sgn}(I_{batt})) \tag{9}$$

During continuous discharge, $H\to -1$, the voltage remains below the equilibrium potential V_{eq}.

C. Polarization Voltage (Dual-RC)

$$\frac{dV_{Ci}}{dt}=-\frac{1}{R_iC_i}V_{Ci}+\frac{1}{C_i}I_{batt},\quad i=1,2 \tag{10}$$

Subsubsection: Effect of Aging on Voltage Hysteresis and Polarization

While voltage hysteresis is primarily introduced to capture the intrinsic charge–discharge asymmetry of lithium-ion batteries, aging mechanisms are known to further amplify this effect. From a physical perspective, the growth of the solid electrolyte interphase SEI layer and the degradation of active material increase the charge-transfer resistance and slow down interfacial kinetics. As a result, a larger overpotential is required to sustain the same current, which manifests macroscopically as enhanced polarization and increased voltage hysteresis during discharge.

In principle, this aging-induced asymmetry could be explicitly modeled by introducing aging-dependent hysteresis parameters or additional state variables. However, such an approach would significantly increase model complexity and introduce parameters that are difficult to identify from typical smartphone-level measurements. Moreover, in the present study, the focus is restricted to monotonic discharge scenarios, where the hysteresis state rapidly converges to a saturated value and does not exhibit pronounced dynamic reversal.

Therefore, an engineering approximation is adopted: the effect of aging on polarization asymmetry is implicitly captured through the aging-dependent ohmic resistance R_0. As internal resistance increases with cycle number, the effective voltage drop and associated polarization losses are magnified, indirectly enhancing the observable hysteresis effect without explicitly modifying the hysteresis dynamics.

This approximation is adopted primarily for numerical robustness. Although simplified, it still captures the dominant influence of aging on terminal voltage behavior.

Aging-induced polarization asymmetry is implicitly captured through the increase of ohmic resistance, while explicit aging-dependent hysteresis dynamics are left for future refinement.

4.4 submodule 4: Thermodynamic coupling

Figure 4-4 illustrates the coupled effect of temperature and cycling aging on the internal resistance R0R_0R0 . Two key nonlinear features can be observed. First, internal resistance increases exponentially as temperature decreases, indicating that low-temperature operation strongly amplifies ohmic losses. Second, aging progressively elevates the entire resistance surface, implying that temperature sensitivity becomes more pronounced as the battery ages.

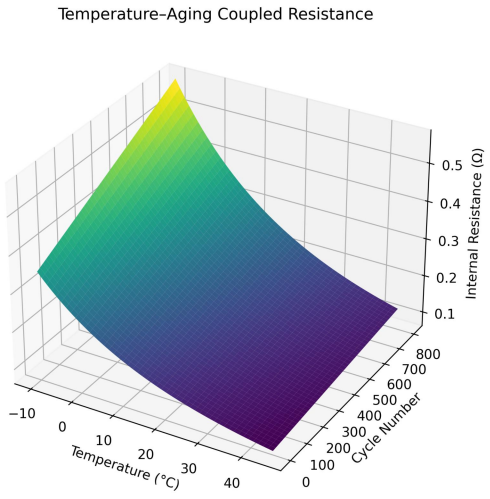

Figure 4-4. R_0 **Temperature-Cycle Surface.**

This coupling helps explain why aged batteries tend to reach voltage collapse much earlier under cold and high-load conditions, even when the remaining capacity appears sufficient.

The system is now internal resistance-dominant, with the battery acting primarily as a heater, not a power source

A. Arrhenius-Aging Coupled Internal Resistance:

This is the core nonlinear source of the model:

$$R_0(T,N_{cyc})=R_{base}\cdot\ R_{aging}(N_{cyc})\cdot\ \exp\left[\frac{E_a}{R_g}\left(\frac{1}{T}-\frac{1}{T_{ref}}\right)\right] \tag{11}$$

B. Heat balance equation:

$$mC_p \frac{dT}{dt} = I_{batt}^2 R_0 - \mathrm{h}A(T - T_{amb}) \tag{12}$$

Thermal parameters are selected to reproduce qualitative trends rather than calibrated absolute temperature profiles. Only the ohmic resistance R_0 is considered as the dominant heat generation source, while polarization losses are neglected for simplicity.

4.5 Power balance constraints and algebraic loop analysis (System Coupling)

Define the effective voltage: $V_{est} = V_{OCV}(SOC,H) - V_{C1} - V_{C2}$。 The algebraic constraint betweenter the minal voltage V_{term} and the current I is as follows:

$$V_{term} = V_{OCV}(SOC,H) - V_{C1} - V_{C2} - I_{batt} R_0(T, N_{cyc}) \tag{13}$$

Combined with the load power demand P_{req} the power balance equation $f(\mathrm{I},\mathbf{x})=0$ is:

$$R_0(T,N_{cyc}) \cdot I_{batt}^2 - [V_{OCV}(SOC,H) - V_{C1} - V_{C2}] \cdot I_{batt} + P_{req}(t) = 0 \tag{14}$$

This relation sits at the center of the model behavior during discharge.The formula is essentially a nonlinear algebraic equation with respect to I_{batt} :

$$f(I_{batt}) = R_0 I_{batt}^2 - V_{est} I_{batt} + P_{req} = 0 \tag{15}$$

The unique solution is:

$$I_{batt} = \frac{V_{est} \pm \sqrt{V_{est}^2 - 4R_0 P_{req}}}{2R_0} \tag{16}$$

From a dynamic perspective, the current I is an implicit function defined by an algebraic equation. The existence of the solution depends on the discriminant:$\Delta = V_{est}^2 - 4R_0 P_{req}$。 The branch with the negative sign must be chosen:

1. Negtive-sign branch: $I^* = \frac{V_{est} - \sqrt{\Delta}}{2R_0}$ corresponds to the low-current, high-voltage operating point, which is the steady-state operating region of the battery.
2. The non-negative branch corresponds to a high-current, low-voltage state, which can lead to positive feedback, resulting in thermal runaway and instantaneous voltage collapse.

The negative branch represents the high-efficiency operational state, whereas the positive branch corresponds to an unstable power-starvation regime where the battery voltage collapse is driven by positive resistive feedback.

When $\Delta \to 0$,the system reach the boundary of the physically feasible region(Discriminant Manifold)at which point the Jacobian with respect to the algebraic variable $\partial f/\partial I$ becomes singular。

Jacobian matrix is: $\frac{\partial f}{\partial I}=2R_0I-V_{est}$

As long as the discriminant $\Delta>0$, then $\left.\frac{\partial f}{\partial I}\right|_{I=I^*}=-\sqrt{\Delta}$, it means that the system is an Index−1 DAE。When the system approaches the critical point ($\Delta \to 0$), it reaches the boundary, and the Jacobian tends to become singular. In numerical simulations, this manifests as strong system stiffness.

The critical point of voltage collapse is analyzed as a saddle-node bifurcation, following the theoretical framework established by Dobson and Chiang[3].

When the two solution branches meet and disappear at $\Delta=0$, this constitutes a typical saddle-node bifurcation. This is equivalent to the numerical representation of a mobile phone "instantly shutting down".

4.6 Numerical Implementation Strategy

As the system approaches the voltage collapse boundary, the DAE becomes stiff, making explicit schemes such as Euler unstable in practice.

The coupled differential–algebraic system is solved using implicit integration schemes (BDF/Radau), which are well-suited for stiff Index-1 DAEs and allow robust handling of near-singular Jacobians.

Event detection is incorporated to terminate simulation when the algebraic power feasibility condition is violated ($\Delta < 0$) or when the terminal voltage reaches the cutoff threshold, corresponding to physical shutdown.

This strategy ensures numerical stability while preserving the correct physical interpretation of instantaneous voltage collapse.

4.7 Multi-scale Aging Evolution Across Discharge Cycles

Aging evolves on a much slower timescale than discharge dynamics and is therefore modeled separately from the fast-time DAE system.

The fast timescale corresponds to discharge time $t \in [0, TTE]$, while aging evolves on the slow cycle index $N \in \mathrm{N}$. Within each discharge, R_0 and $Q_{\max}$ are treated as quasi-static.

Capacity fade follows a square-root law associated with SEI growth:

$$Q_{\max}(N) = Q_{\max}(0)\left(1 - k_Q\sqrt{N}\right) \tag{17}$$

Internal resistance growth is approximated linearly for numerical stability:

$$R_0(N) = R_0(0)\left(1 + k_R N\right) \tag{18}$$

At the beginning of each discharge simulation, the aging parameters are updated according to the slow-time aging laws, and then held constant during the fast-time DAE integration. Fully coupled multi-scale aging DAEs are beyond the scope of this work.

$$Q_{\max}^{(k+1)} = Q_{\max}^{(k)}\left(1 - k_Q\sqrt{\Delta N_k}\right), R_0^{(k+1)} = R_0^{(k)}\left(1 + k_R \Delta N_k\right), \tag{19}$$

In practice, aging parameters are updated discretely between discharge cycles and treated as quasi-static during each fast-time DAE simulation.

5. Test the Models

Algorithm 1 Cycle-Aware Battery Discharge Simulation

Input: Initial SOC_0, initial capacity $Q_{\max}^{(0)}$, initial resistance $R_0^{(0)}$, number of cycles N_{cyc}

Output: Time-to-empty $\mathrm{TTE}^{(k)}$, critical SOC $\mathrm{SOC}_{\mathrm{crit}}^{(k)}$, and shutdown mode for each cycle

1: **for** $k = 1, \ldots, N_{\mathrm{cyc}}$ **do**
2: Update aging parameters:
$Q_{\max}^{(k)} \leftarrow \mathcal{A}_Q\left(Q_{\max}^{(k-1)}\right),\ R_0^{(k)} \leftarrow \mathcal{A}_R\left(R_0^{(k-1)}\right)$
3: Initialize fast-time states $(\mathrm{SOC}, t, V_{c1}, V_{c2})$
4: **while** power feasibility condition $\Delta > 0$ is satisfied **do**
5: Solve algebraic power constraint for current I
6: Integrate the coupled DAE system over one time step
7: **end while**
8: Record $\mathrm{TTE}^{(k)}$, $\mathrm{SOC}_{\mathrm{crit}}^{(k)}$, and shutdown mode
9: **end for**

Figure 5-0 Partial Code

5.1 Stability & Phase Plane Analysis

When examining the boundary of an “instantaneous crash”, it is not sufficient to treat it as a numerical artifact.

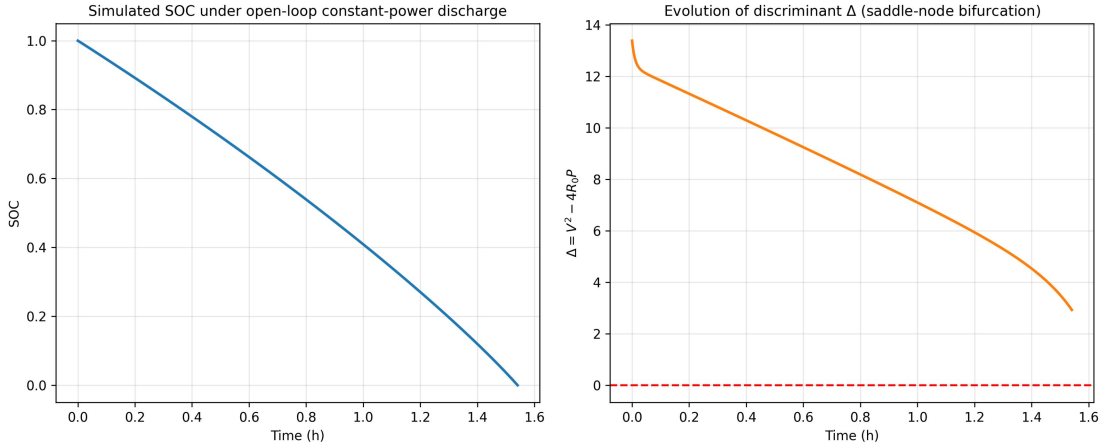

Figure 5-1-1. DAE SOC and Discriminant Open-Loop.

Note that Δ remains positive at SOC≈0 for this specific P_{base}, implying the cut-off is energy-limited rather than stability-limited.

A. Discriminant Manifold

Numerical simulations demonstrate that during open-loop constant power discharge, the discriminant Δ progressively approaches the critical value 0 as the state of charge (SOC) diminishes, thereby validating the physical significance of the discriminant manifold as the boundary of the system's dynamic feasible region.

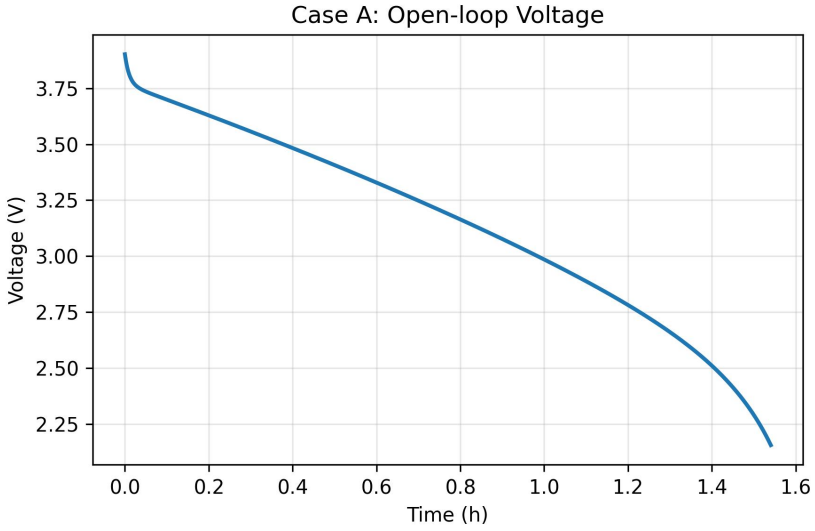

Figure 5-1-2. Voltage Collapse Open-Loop.

The simulation shows the rapid terminal voltage decline under a high-power demand (P_{base}=8W). The absence of feedback leads the system directly toward the singular manifold Δ=0.

For quadratic equation, the solvable condition of physics is Δ≥0. Define the Breakthrough boundary: in the system state space:

$$\Delta(SOC,T,N_{cyc})=[V_{est}(SOC)]^2-4\cdot R_0(T,N_{cyc})\cdot P_{req} \quad (20)$$

Where $V_{est}=V_{OCV}-V_{pol}$ denotes the effective voltage after accounting for the ohmic voltage drop.

B. Phase Plane Visualization

Plot the safe operating region for different aging levels and temperatures with SOC as the x-axis and load power P as the y-axis.

To prevent the system from exceeding the crash threshold P_{crit}, the closed-loop current-limiting mechanism dynamically adjusts the load power, ensuring the discriminator Δ remains in the positive range.

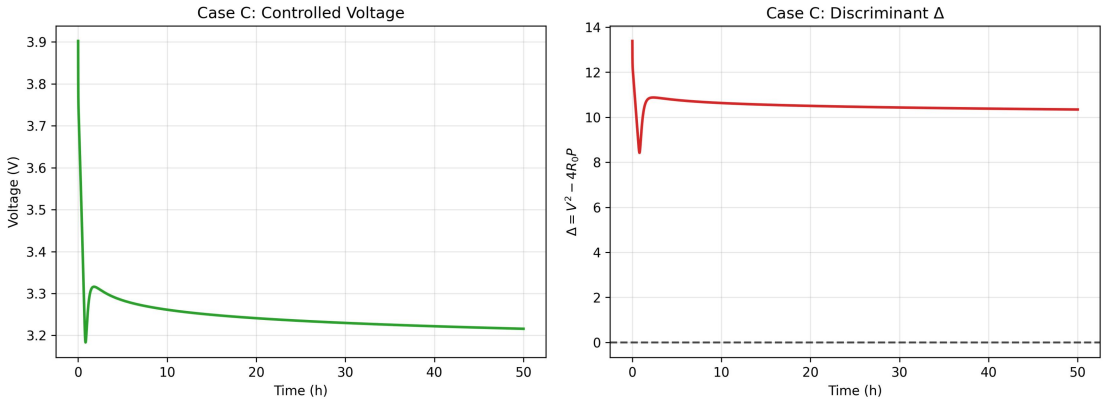

Figure 5-1-3. Voltage and Discriminant Controlled.

The feedback controller acts as a singular perturbation buffer, preventing the state trajectory from hitting the singular manifold where $\partial f/\partial I$=0. The feedback mechanism effectively regularizes the power demand. Note that the discriminant Δ is stabilized above zero, effectively preventing the saddle-node bifurcation and extending the operational duration (Case C).

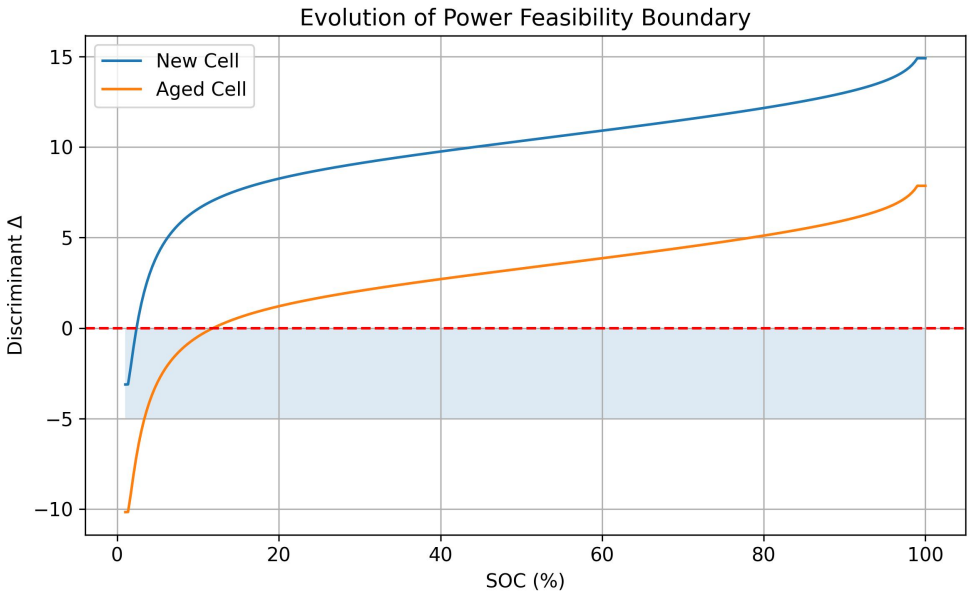

Figure 5-1-4. Discriminant Boundary vs SOC.

In phase-plane analysis, polarization voltages are neglected to highlight the dominant effect of ohmic resistance and OCV.

curvilinear equation: $P_{crit}(SOC)=\frac{V_{est}(SOC)^2}{4R_0(T)}$

Analysis: The area below the curve represents the stable operation zone
The voltage collapse region is above the curve.

As N_{cyc} increases,R_0 grows,the curve shifts downward overall, and the SOAarea contracts sharply.

As aging progresses or temperature decreases, the safe operating area SOA shrinks significantly, explaining the observed sudden shutdown phenomena under high-load applications such as mobile gaming.

The DAE-based simulation can be interpreted as a numerical realization of the SOC-domain integral defining the discharge time.

5.2 Simulation process and result definition

The remaining discharge time TTE can be theoretically defined as the time required for the state of charge to evolve from its initial value SOC_0 to the critical shutdown state.

Given that the battery current is not an externally prescribed input but an implicit function of the system states through the algebraic power balance constraint, the discharge time can be expressed as

$$TTE=\int_{SOC_{crit}}^{SOC_0} \frac{Q_{max}}{I^*(SOC,T,N)},dSOC \tag{21}$$

where I denotes the physically stable branch of the algebraic current solution.

In practice, this integral does not admit a closed-form solution due to the strong nonlinear coupling among SOC, temperature, aging, and power feedback. Therefore, TTE is evaluated numerically by integrating the coupled DAE system until the shutdown condition is met.

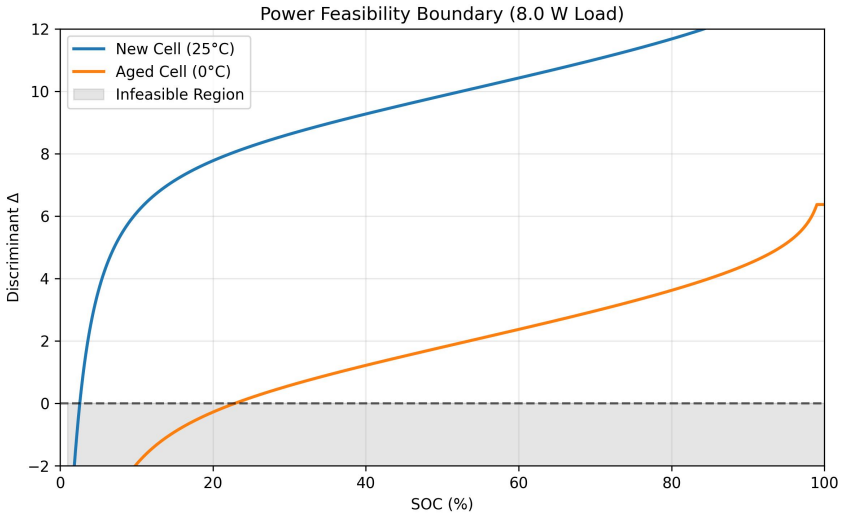

Figure 5-2. Power Feasibility Boundary P=8W.

Forecast indicator output:

1. **TTE (Time-to-Empty)**: $\inf\{t:SOC=0 \vee V_{term} \leq 3.0V \vee \Delta<0\}$

Once the terminal voltage approaches the soft shutdown threshold, the feedback controller gradually reduces the power demand, preventing immediate voltage collapse. This behavior cannot be captured by traditional open-loop discharge models.

2. **Power-off type determination**:

Energy depletion: $SOC \approx 0$ and $V_{term} > 3.0V$。
low voltage protection: $V_{term} \leq 3.0V$ and $\Delta>0$ (common in aged batteries) 。
Instant crash: $\Delta<0$ (Commonly observed in low temperatures + heavy loads) 。

6. Sensitivity Analysis

To quantitatively evaluate the system's robustness under various operating conditions, this section analyzes the dimensionless sensitivity of residual time to discharge (TTE) to internal resistance R_0 perturbations;Since the endpoint of TTE is

determined by the critical state SOC_{crit} defined by the power criterion Δ=0, the relative sensitivity coefficient S_{R_0} of SOC_{crit} with respect to R_0 is defined as: S_{R_0}:

$$S_{R_0}=\frac{\partial SOC_{crit}/SOC_{crit}}{\partial R_0/R_0}=\frac{R_0}{SOC_{crit}}\cdot\frac{dSOC_{crit}}{dR_0} \tag{22}$$

6.1 Implicit function differentiation

by algebraic constraints $f(SOC,R_0)=V_{OCV}(SOC)^2-4R_0P_{req}=0$, Use implicit function for differentiation:

$$\frac{dSOC_{crit}}{dR_0}=-\frac{\partial f/\partial R_0}{\partial f/\partial SOC}=\frac{4P_{req}}{2V_{OCV}(SOC)\cdot\frac{dV_{OCV}}{dSOC}} \tag{23}$$

Analysis of this equation reveals that the sensitivity magnitude is highly dependent on the slope of the V_{OCV}curve at the critical point and the current voltage level. In regions with lower SOC, the V_{OCV} decreases rapidly, resulting in a nonlinear increase in $dSOC_{crit}/dR_0$.

6.2 Sensitivity thermal analysis

The distribution of S_{R_0} was calculated through analyzing the parameter space defined by temperature T∈[−10,45]◦ C and aging cycles N_{cyc} ∈[0,800].

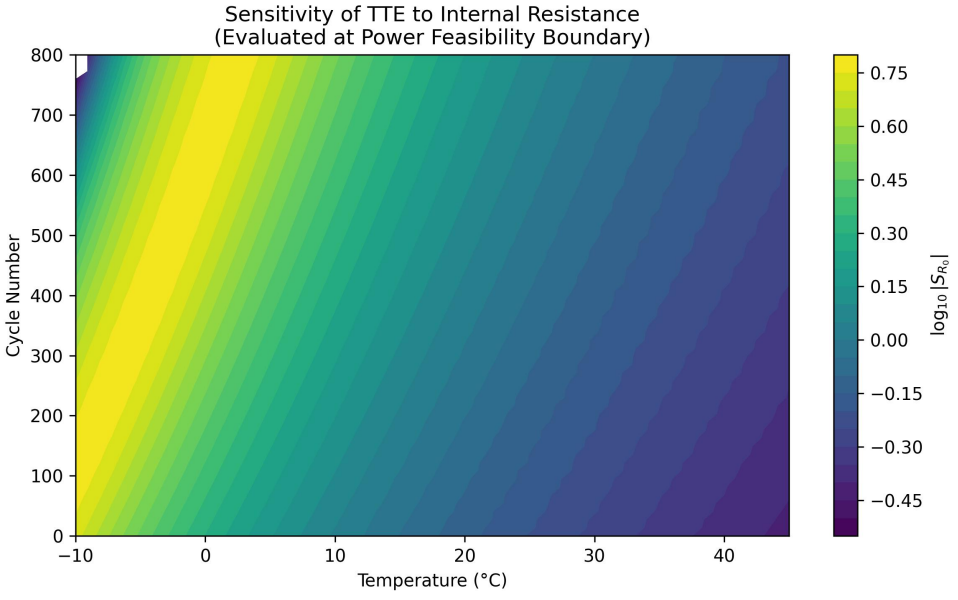

Figure 6-2. Sensitivity TTE vs R0

The logarithmic scale $\log_{10}|S_{R_0}|$ was used for visualization.

1. **Low Sensitivity Region**: At room temperature and when the battery is new, the internal resistance is low, the system is far from the saddle node bifurcation point, and S_{R_0} remains at a low level. The TTE error mainly originates from the maximum capacity $Q_{\max}$.
2. **High Sensitivity Region**: As the temperature decreases or the aging process intensifies,The exponential growth of R_0 drives the system toward the boundary of the physically feasible region. The sensitivity coefficient in the low-temperature aging zone exhibits a magnitude shift ($\log_{10}|S_{R_0}|>1$).This observation helps clarify why traditional Coulomb counting often performs poorly for aged batteries. It is recommended that the Battery Management System (BMS) should increase the internal resistance update frequency at low temperatures or during the end of aging.

6.3 Aging-Dependent Performance Metrics

1. Critical SOC

$$SOC_{crit}(N)=\min SOC \mid \Delta(SOC,T,N)=0 \tag{24}$$

2. Critical Power

$$P_{crit}(N)=\frac{V_{est}^2(SOC_{crit})}{4R_0(N)} \tag{25}$$

3. Shutdown Mode Ratio

$$\Gamma(N)=\frac{N_{\Delta<0}}{N_{total}} \tag{26}$$

7. Strengths and Weakness

7.1 Strengths:

（1）Mechanistic and dynamically consistent formulation.

The proposed Index-1 DAE framework captures the coupled electrochemical, thermal, and electrical dynamics governing power feasibility in aging lithium-ion batteries.

（2）Explicit characterization of power collapse.

Voltage collapse is identified as a saddle-node bifurcation of the algebraic power constraint, enabling quantitative prediction of critical operating boundaries.

7.2 Weakness:

Modeling simplifications for tractability.

To ensure numerical tractability and real-time feasibility, the battery is modeled as a spatially lumped system with chemistry-dependent parameters. As a result, spatial heterogeneity and high-rate diffusion effects are neglected, and limited parameter calibration is required when adapting the model to different cell chemistries or manufacturers. These simplifications may introduce deviations under extreme discharge conditions but do not affect the model's ability to capture system-level stability boundaries and voltage collapse behavior.

8. Conclusion and Recommendations

8.1 Conclusion:

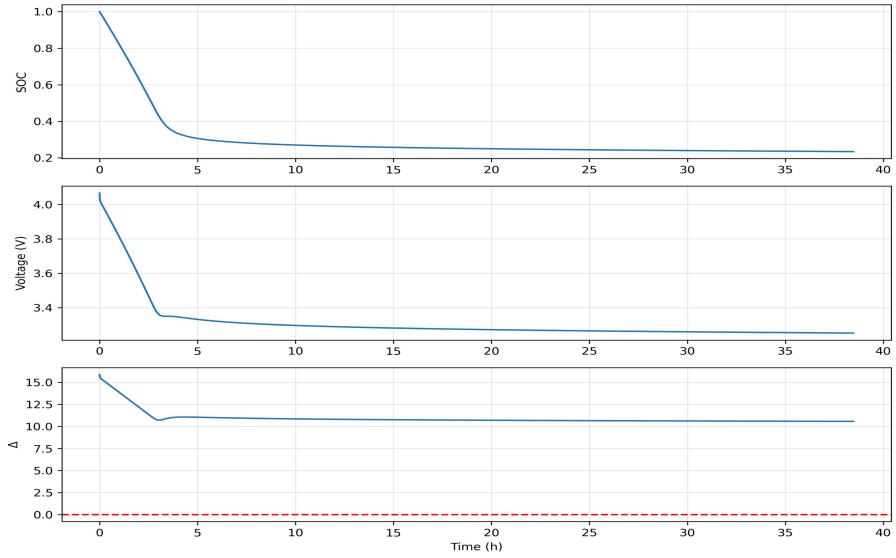

Figure 8-1 terminal voltage-time evolution curve

(1) The proposed Index-1 DAE model brings electro-thermal effects, aging, and closed-loop feedback into a single discharge description.

(2) Aging analysis indicates that moderate capacity loss can lead to disproportionate TTE reduction under heavy load, with internal resistance growth playing a dominant role in system instability.

(3) Phase-plane analysis reveals the shrinking safe operating region under combined effects of aging, low temperature, and high load.

8.2 Recommendations:

Based on the discriminant-based stability analysis, several high-level recommendations are derived for battery-aware system design.

1. "Downgrading" strategy in low-temperature environments:

The model shows that the internal resistance R_0 of the battery will increase exponentially when the temperature is below 0°C.

2. Maintain light usage when battery level is low:

As the SOC decreases, V_{OCV} will also decrease accordingly, This will make the $V_{est}^{\ 2}$ in the discriminator smaller.

3. Recognizing the "Illusion of Aging":

Model display,As the number of cycles N_{cyc} increases,The R_0 growth rate is much greater than the attenuation of capacity Q on the reduction of TTE.

Aging-induced internal resistance growth has a more pronounced impact on effective power availability than capacity fade, explaining the perceived “illusion of aging” under high load.

1. Introduction of DAE-based real-time power budget

Strategy: The proposed DAE framework enables real-time estimation of power feasibility boundaries, which could inform proactive power budgeting strategies in future battery management systems.

2. The thermal throttling perception described below:

Strategy: Utilize the heat balance equation $mC_p \frac{dT}{dt}$ in the model.

3. The Honest Time to Eat (TTE) shows optimization:

Strategy: Update the SOC and time prediction on the UI.

The model also supports an “honest TTE” estimation by predicting termination due to power infeasibility rather than energy depletion, addressing limitations of traditional Coulomb-counting-based indicators.

References

[1] B. Saha and K. Goebel, “Battery Data Set,” *NASA Ames Prognostics Data Repository*, NASA Ames Research Center, Moffett Field, CA, 2007. [Online]. Available: https://www.nasa.gov/intelligent-systems-division/discovery-and-systems-health/pcoe/pcoe-data-set-repository/

[2] M. Pecht, “CALCE Battery Data,” *Center for Advanced Life Cycle Engineering (CALCE)*, University of Maryland, 2023. [Online]. Available: https://calce.umd.edu/battery-data

[3] I. Dobson and H.-D. Chiang, “Towards a theory of voltage collapse in electric power systems,” *Systems & Control Letters*, vol. 13, no. 3, pp. 253-262, 1989.

[4] L. Zhang et al., “Accurate online power estimation and automatic battery behavior based power model generation for smartphones,” in *Proc. IEEE/ACM/IFIP Int. Conf. Hardware/Software Codesign and System Synthesis (CODES+ISSS)*, 2010.

[5] Google, “Android Power Management and Thermal Mitigation Strategy,” *Android Open Source Project (AOSP) Documentation*, 2024. [Online]. Available: https://source.android.com/docs/core/power.

Appendix

```
def get_ocv(soc):
    soc = np.clip(soc, 1e-3, 1.0 - 1e-3)
    return 3.5 + 0.45*soc - 0.04/soc - 0.08*np.log(1 - soc)
def get_internal_params(T_celsius, N_cyc):
    R_base, beta, Ea, Rg, T_ref = 0.12, 8e-4, 2e4, 8.314, 298.15
    Tk = T_celsius + 273.15
    R_aging = 1.0 + beta * N_cyc
    R0 = R_base * R_aging * np.exp(Ea / Rg * (1.0/Tk - 1.0/T_ref))
    Q_max = 4.0 * (1 - 0.025 * np.sqrt(N_cyc/100)) * 3600 # As
    return R0, Q_max
def get_throttling_factor(v_term, T_c, V_crit=3.25, T_crit=45.0):
    l_t = 1.0 / (1.0 + np.exp((T_c - T_crit) / 2.0))
    l_v = 0.5 * (1.0 + np.tanh(4.0 * (v_term - V_crit)))
    return min(l_t, l_v)
def run_tte_simulation(p_base, T_amb, N_cyc):
    dt, soc, vc1, T = 1.0, 1.0, 0.0, T_amb
    R0, Q_max = get_internal_params(T_amb, N_cyc)
    history = {'t':[], 'soc':[], 'v':[], 'delta':[]}
    t = 0
    while soc > 0:
        v_est = get_ocv(soc) - vc1
        p_req = p_base * get_throttling_factor(v_est, T)
        i_batt, delta = solve_current_dae(v_est, p_req, R0)
        if i_batt is None: break
        # State Evolution (DAE Integration)
        soc -= (i_batt * dt) / Q_max
        vc1 += dt * (-vc1/(0.02*2500) + i_batt/2500)
        T   += dt * (i_batt**2 * R0 - 0.5*(T-T_amb)) / 500
        v_term = v_est - i_batt * R0
        if v_term < 3.0: break
        for k, v in zip(history.keys(), [t/60, soc, v_term, delta]):
            history[k].append(v)
        t += dt
    return history
def calculate_sensitivity_s_r0(soc_crit, T, N, P_req, epsilon=0.01):
    def find_boundary_soc(r_scale):
        soc_range = np.linspace(0.01, 0.99, 1000)
        R0, _ = get_internal_params(T, N)
        delta = get_ocv(soc_range)**2 - 4 * (R0 * r_scale) * P_req
        idx = np.where(delta > 0)[0]
        return soc_range[idx[0]] if len(idx) > 0 else 1.0
    s0 = find_boundary_soc(1.0)
    s1 = find_boundary_soc(1.0 + epsilon)
    return ((s1 - s0) / (s0 + 1e-6)) / epsilon
```

Report on Use of AI Tools

AI tools: Deepseek, Doudou

Usage overview:

1. Use AI to polish and translate the paper.

Given the linguistic disparities, artificial intelligence was employed to bridge the communication gaps. Specifically, AI was utilized to refine and translate sections such as the summary and question analysis in the papers, ensuring enhanced linguistic precision without compromising the inherent validity of our model.;

2. With the help of AI, the code was analyzed and improved.

While drawing inspiration from GitHub projects,We implemented minor code optimizations using AI,but it does not affect our original reasonable model and hypothesis;